Sources of uncertainty in modeled land carbon storage within and across three MIPs: Diagnosis with three new techniques

Sha Zhou[1], Junyi Liang[2], Xingjie Lu[3,2], Qianyu Li[4,2], Lifen Jiang[3], Yao Zhang[5], Christopher R. Schwalm[6,7], Joshua B. Fisher[8], Jerry Tjiputra[9], Stephen Sitch[10], Anders Ahlström[11,12], Deborah N. Huntzinger[13], Yuefei Huang[1,14], Guangqian Wang[1], Yiqi Luo[3,4]

[1]State Key Laboratory of Hydroscience and Engineering, Department of Hydraulic Engineering, Tsinghua University, Beijing 100084, China

[2]Department of Microbiology and Plant Biology, University of Oklahoma, Norman, OK 73019, USA

[3]Center for Ecosystem Sciences and Society, Department of Biological Sciences, Northern Arizona University, Flagstaff, Arizona, USA

[4]Department of Earth System Science, Tsinghua University, Beijing 100084, China

[5]Department of Microbiology and Plant Biology, Center for Spatial Analysis, University of Oklahoma, Norman, OK 73019, USA

[6]Woods Hole Research Center, Falmouth MA 02540, USA

[7]Center for Ecosystem Science and Society, Northern Arizona University, Flagstaff AZ 86011, USA

[8]Jet Propulsion Laboratory, California Institute of Technology, 4800 Oak Grove Drive, Pasadena, CA, 91109, USA

[9]Uni Research Climate, Bjerknes Centre for Climate Research, Bergen, Norway

[10]College of Life and Environmental Sciences, University of Exeter, Amory Building, Rennes Drive, Exeter, EX4 4RJ, UK

[11]Department of Earth System Science, Stanford University, Stanford, California, USA

[12]Department of Physical Geography and Ecosystem Science, Lund University, Lund, Sweden

[13]School of Earth Sciences and Environmental Sustainability and the Department of Civil Engineering, Construction Management, and Environmental Engineering, Northern Arizona University, P.O. Box 5694, Flagstaff, Arizona, USA

[14]College of Ecological and Environmental Engineering, Qinghai University, Xining 810086 Qinghai, China

Corresponding author address:

Sha Zhou (zhous13@mails.tsinghua.edu.cn)

State Key Laboratory of Hydroscience and Engineering, Tsinghua University, Beijing 100084, China

Yiqi Luo (luoyiqi@mail.tsinghua.edu.cn)

Department of Earth System Science, Tsinghua University, Beijing 100084, China

Abstract

Terrestrial carbon cycle models have incorporated increasingly more processes as a means to achieve more realistic representations of ecosystem carbon cycling. Despite this, there are large across-model variations in the simulation and projection of carbon cycling. Several model inter-comparison projects (MIPs), e.g., CMIP5 (historical simulations), TRENDY, and MsTMIP, have sought to understand inter-model differences. In this study, we developed a suite of new techniques to conduct post-MIP analysis to gain insights into uncertainty sources across 25 models in the three MIPs. First, terrestrial carbon storage dynamics were characterized by a three-dimensional (3D) model output space with coordinates of carbon residence time, net primary productivity (NPP), and carbon storage potential. The latter represents the potential of an ecosystem to lose or gain carbon. This space can be used to measure how and why model output differs. Models with a nitrogen cycle generally exhibit lower annual NPP in comparison with other models, and mostly negative carbon storage potential. Second, a transient traceability framework was used to decompose any given carbon cycle model into traceable components, and identify the sources of model differences. The carbon residence time (or NPP) was traced to baseline carbon residence time (or baseline NPP related to the maximum carbon input), environmental scalars, and climate forcing. Third, by applying a variance decomposition method, we show that the inter-model differences in carbon storage can be mainly attributed to the baseline carbon residence time and baseline NPP (> 90% in the three MIPs). The three techniques developed in this study offer a novel approach to gain more insight from existed MIPs and can point out directions for future MIPs. Once the sources of uncertainties among models are identified, we can effectively improve models by prioritizing future research efforts on assessing the model performance at the specified mechanism-level.

1. Introduction

To understand better the past, present, and future role of the terrestrial biosphere in the global carbon cycle, terrestrial carbon cycle models have become increasingly complex. These models are continuously developed and updated based on improved understanding of mechanisms controlling the carbon cycle, such as the improvement of Community Land Model (Oleson et al., 2013). Compared to the Coupled Climate-Carbon Cycle Model Inter-comparison Project (C^4MIP) (Friedlingstein et al. 2006), the fifth phase of the Coupled Model Inter-comparison Project (CMIP5) comprises models that include improved processes, components, or forcing (Knutti and Sedláček 2012; Taylor et al. 2012). However, large uncertainties remain in the simulation and prediction of carbon uptake and storage among different models. The simulated global soil carbon varied by 5.9 fold across 11 models from CMIP5, resulting from the difference in the simulated net primary productivity and the parameterization of soil heterotrophic respiration (Todd-Brown et al. 2013), as well as the integration over long spin-up procedures (Exbrayat et al. 2014). To improve future projection of carbon storage dynamics and constrain its uncertainties, it is essential to understand the underlying key mechanisms of the global carbon cycle.

Model inter-comparison studies have been conducted to assess differences between model output and explain the uncertainties among models (Fisher et al. 2014; Friend et al. 2014; Nishina et al. 2014; 2015). Schwalm et al. (2010) examined the ability of 22 terrestrial biosphere models to simulate the seasonal variability in biosphere-atmosphere exchange of CO_2 using data from 44 flux tower sites. Model performance was generally poor, and a large divergence between observations and simulations (~10 times observational error) was found, especially for non-

forested sites. Keenan et al. (2012) compared the inter-annual variability of CO_2 exchange from 16 terrestrial biosphere models against 11 long-term eddy-covariance forest sites in North America. They found that the large biases in the modeled inter-annual variability are related to the poor representation of spring phenology, soil thaw and snowpack melting, and the lagged response to extreme climatic events. Ichii et al. (2010) showed that the terrestrial biosphere models, which have been calibrated using eddy flux data can successfully capture the seasonal and inter-annual variations in the terrestrial carbon cycle, indicating that the eddy flux observations are critical to improve model simulations and reduce uncertainties. Although observations can evaluate model performance and constrain model uncertainties to a certain degree, the sources of uncertainties among models are still hard to quantify (De Kauwe et al. 2014).

Several model inter-comparison projects (MIPs) have been established to identify the sources of model uncertainties and improve process representation in models. The Coupled Model Inter-comparison Project (CMIP) provides a standard experiment protocol to evaluate output from coupled ocean-atmosphere-cryosphere-land general circulation models (Meehl et al. 2005). One of the most important targets of the fifth phase of the CMIP (CMIP5) is to assess the mechanisms responsible for the spread in model projections when a same set of "external" forcing, such as greenhouse gas forcing in historical simulations, is used (Taylor et al. 2012). The TRENDY (Trends in net land atmosphere carbon exchange over the period 1980-2009) (Sitch et al. 2015), and MsTMIP (Multi-scale Synthesis and Terrestrial Model Inter-comparison Project) (Huntzinger et al. 2013; Wei et al. 2014) projects facilitate the comparison of model output by using prescribed environmental and meteorological drivers shared among all models. Thus, the role of model structure and parameters in the uncertainty of land-atmosphere carbon

exchange can be systematically evaluated. For instance, by investigating the difference in model output under a series of common scenarios, the contribution of environmental drivers (e.g., changing CO_2, climate, nitrogen, and land use) to the trend and variability of carbon exchange can be diagnosed (Ahlström et al., 2012; Nishina et al., 2015). Despite these projects can evaluate the impact of environmental drivers on carbon storage based on sensitivity simulations, they have led to little understanding of the underlying mechanisms of carbon storage variations across different models. Even so, the simulated terrestrial carbon storage dynamics from these MIPs can be used to identify the sources of inter-model differences.

Based on the biogeochemical principles of the terrestrial carbon cycle, Xia et al. (2013) proposed a framework to decompose a complex carbon cycle model into traceable components. In the framework, the modeled ecosystem carbon storage capacity is decomposed into the product of carbon residence time and net primary productivity (NPP). The carbon residence time refers to the mean duration of carbon in terrestrial ecosystems from its input via photosynthesis to its release via respiration (Luo et al. 2003). A three-dimensional (3D) model output space proposed by Luo et al. (2017) extends the approach of Xia et al. (2013) by involving carbon storage potential to represent the difference between carbon storage capacity and carbon storage itself. The 3D model output space can be used to evaluate the terrestrial carbon storage dynamics by decomposing the carbon storage into carbon residence time, NPP, and carbon storage potential. Thus, the simulated terrestrial carbon storage can be placed into the 3D model output space to attribute differences in model outputs to the three variables.

The three variables can be further decomposed into their traceable components to track the sources of model uncertainty. The traceability framework developed by Xia et al. (2013) suggested that the carbon residence time can be traced to 1) baseline carbon residence time,

129 which is related to vegetation characteristics and soil types, 2) environmental scalar, including
130 temperature and water scalars, and 3) climate variables, such as temperature and precipitation.
131 The baseline carbon residence time is inversely related to the maximum decomposition rate,
132 which is modified by temperature and moisture conditions. The environmental scalar expressed
133 as a function of environmental variables, such as temperature and precipitation, links the baseline
134 carbon residence time to actual carbon residence time. This framework decomposes carbon
135 residence time into its traceable components, however, the traceability analysis for NPP has not
136 been performed.

137 In terrestrial carbon cycle models, NPP is generally estimated using two basic
138 approaches. Most models, such as BIOME-BGC (Running and Hunt, 1993) and HYBRID
139 (Friend et al., 1997), estimate NPP as the difference between gross primary productivity (GPP)
140 and autotrophic respiration (Ra); while the others directly simulate NPP as influenced by
141 vegetation and environmental variables, such as CASA (Potter et al. 1993) and CENTURY
142 (Parton 1996). Despite different representations of physical and biological processes in different
143 models, the concept of light use efficiency (LUE) underpins the simulation of NPP across most
144 models (Cramer et al. 1999). That is, NPP (or GPP) can be expressed as the product of LUE,
145 photosynthetically active radiation (PAR), and the fraction of PAR absorbed by vegetation
146 (fPAR). LUE is regulated by climatic conditions (e.g., temperature and precipitation), and fPAR
147 is the most important vegetation characteristics in controlling potential photosynthetic capacity
148 of vegetation (Schloss et al. 1999). Thus, NPP can be traced to a "baseline NPP" which is related
149 to vegetation characteristics and an environmental scalar determined by environmental variables,
150 in a similar fashion to carbon residence time. The baseline NPP corresponds to the maximum
151 carbon input when the environmental conditions are favorable for carbon assimilation. The

environmental stress on NPP is evaluated by the environmental scalar, which converts the baseline NPP to actual NPP. Following this traceability analysis, the variation in terrestrial carbon storage can be quantitatively attributed to its sources to evaluate the inter-model differences based on variance decomposition.

The objective of this study is to compare the annual carbon storage simulated by different models in the three MIPs, i.e., CMIP5, TRENDY and MsTMIP, based on the 3D model output space, and identify the sources of carbon storage variation using a transient traceability framework and a variance decomposition method. First, the terrestrial carbon storage is decomposed into the 3D model output space: carbon residence time, NPP, and carbon storage potential. Second, a transient traceability framework of carbon storage dynamics is proposed to determine what controls the carbon cycle dynamics, e.g., climate factors such as temperature and precipitation. Following the transient traceability framework, the sources of the variation in carbon storage dynamics will be diagnosed. Third, the variation in carbon storage simulations is attributed to its sources by quantifying the relative contributions of them using the variance decomposition method. Our rigorous framework for multi-model assessment facilitates better understanding of the complex behaviors of various terrestrial carbon cycle models, and is suggested to be a valuable evaluation method for future model inter-comparison projects.

2. Methods and Materials

a. Carbon storage dynamics decomposition

Based on mathematical analysis of the matrix equation for terrestrial carbon cycle models, Luo et al. (2017) developed a three-dimensional (3D) model output space to assess the

dynamics of terrestrial carbon storage (X). By decomposing the carbon storage dynamics into three variables, we can better evaluate the responses of terrestrial carbon storage to environmental factors and the capability of ecosystem processes to influence the carbon storage change.

The magnitude and direction of carbon storage change are controlled by the carbon storage capacity (X_c), i.e., the capacity of an ecosystem to store carbon or the carbon storage at steady-state under current conditions (see Table 1 for symbol definition). X_c is jointly determined by the carbon residence time (τ_E) and ecosystem carbon input, e.g., net primary productivity (NPP) (Xia et al. 2013).

$$X_c = \tau_E NPP \quad (1)$$

Luo et al. (2017) further proposed that the capability of the terrestrial carbon cycle to influence carbon storage can be evaluated by carbon storage potential (X_p), the potential of an ecosystem to store additional carbon or lose carbon. X_p is proportional to the rate of carbon storage change ($X^{'}$), and regulated by the chasing time (τ_{ch}).

$$X_p = \tau_{ch} X^{'} \quad (2)$$

τ_{ch} is a non-negative matrix of carbon residence times through the network of individual pools. X_p is positive/negative when the carbon storage capacity is larger/smaller than current the carbon storage. Positive X_p values indicate an increasing trend of carbon storage, and vice versa. The larger the carbon storage potential, the faster the rate of carbon storage change, and the ratio between the two is determined by the chasing time.

194 Carbon storage can be expressed as the difference between carbon storage capacity
195 (equation (1)) and carbon storage potential (Luo et al. 2017). Thus, dynamics in terrestrial carbon
196 storage can be projected into a 3D model output space: τ_E, NPP, and X_p as

197 $$X = \tau_E NPP - X_p \quad (3)$$

198 The 3D model output space above offers a new framework to quantify differences across land
199 carbon cycle models. Thus, it helps us to understand better complex model dynamics, diagnose
200 sources of model differences, and improve model predictive capability.

201 To apply the 3D model output space to those three MIPs, we consider the terrestrial
202 ecosystem as one pool. According to Luo et al. (2017), τ_{ch} equals to τ_E when there is only one
203 pool. Thus, equation (3) can be transformed into

204 $$X = \tau_E(NPP - X^{'}) \quad (4)$$

205 where $(NPP - X^{'})$ represents the total carbon losses from the terrestrial ecosystem, mainly
206 through heterotrophic respiration. Generally, X and NPP are directly available from model
207 output, $X^{'}$ can be calculated as the difference of carbon storage between time step (t+1) and t. So
208 the carbon residence time and carbon storage potential can be calculated as follows:

209 $$\tau_E = \frac{X}{NPP - X^{'}} \quad (5a)$$

210 $$X_p = \tau_E NPP - X \quad (5b)$$

211 Although the structure varies in different models, a one-pool model can effectively estimate the
212 three variables. For example, we have reproduced the model output in CanESM2 and CESM1-

213 BGC using a five-pool model, and found that the derived τ_E is close to that calculated using the
214 one-pool model (Fig. S1).

215

216 *b. Traceability analysis of carbon storage dynamics*

217 Xia et al. (2013) developed a framework for traceability analysis of steady-state carbon
218 storage. This study expands the framework to transient dynamics of terrestrial carbon storage
219 (Fig. 1), by incorporating the third dimension of carbon cycle dynamics, i.e., the carbon storage
220 potential. This transient traceability framework can decompose the land carbon cycle into
221 traceable components. The framework first traces the simulated terrestrial carbon storage to
222 carbon storage capacity and potential. The former can be traced to a product of carbon residence
223 time and NPP. The carbon residence time and NPP are further traced to (1) their baseline values,
224 which are determined by soil properties and vegetation characteristics, (2) the environmental
225 scalars, including temperature and water scalars, and ultimately (3) the climate forcing.

226

227 1) Traceability analysis for carbon residence time and NPP

228 The carbon residence time is mainly related to carbon release from an ecosystem via
229 decomposition and respiration. The maximum carbon decomposition rate corresponds to the
230 baseline carbon residence time, under optimal temperature and moisture conditions (Xia et al.
231 2013). The carbon residence time is determined by the baseline carbon residence time ($\tau_E{}'$) and
232 modified by the environmental scalar (ξ).

233 $$\tau_E = \xi^{-1}\tau_E{}' \quad (6)$$

234 The baseline carbon residence time is usually preset in a carbon cycle model, according to soil
235 properties and vegetation characteristics (Fig. 1).

236 NPP has been simulated according to different processes by different models, and a large
237 uncertainty of modeled NPP simulation still exists (Cramer et al. 1999; Schwalm et al. 2010).
238 Almost all models simulate NPP as controlled by vegetation characteristics and regulated by
239 climate variables (Schloss et al. 1999). We assume a "baseline NPP" which is related to the
240 maximum carbon input when the environmental conditions are favorable for carbon assimilation,
241 and an environmental scalar to convert the baseline NPP to actual NPP. Thus, the modeled NPP
242 can be traced to baseline NPP ($NPP^{'}$) and an environmental scalar (δ), just as the carbon
243 residence time, for the sake of this analysis:

244 $$NPP = \delta NPP^{'} \quad (7)$$

245 The baseline NPP is related to vegetation characteristics, including photosynthetic capacity and
246 vegetation type (Fig. 1).

247 The environmental scalar usually consists of the temperature and water scalars, which are
248 traced to the climate forcing, i.e. temperature and precipitation. The terrestrial carbon storage is
249 affected by various environmental factors, including climate, CO_2 concentration, land cover,
250 nitrogen deposition, etc. In this study, we focus on the effect of climate change on the carbon
251 storage, by investigating the responses of carbon residence time and NPP to climate forcing, i.e.,
252 temperature and precipitation. Thus, the environmental scalars ξ and δ are further decomposed
253 into temperature and water scalars as:

254 $$\xi = \xi_T \xi_W \quad (8a)$$

255 $$\delta = \delta_T \delta_W \quad (8b)$$

where the subscripts T and W refer to the temperature and water scalars, respectively.

To estimate the baseline residence time and baseline NPP, we use an optimization method to reproduce the simulation results of carbon residence time and NPP using annual scale temperature and precipitation as inputs. Here we only show the optimization method for the carbon residence time; the method for NPP is the same. In this method, $\tau_E^{'}$ is set to be an unknown parameter, ξ_T and ξ_W are expressed as functions of temperature (T) and precipitation (W), respectively.

$$\xi_T = Q_{10}^{\left(\frac{T - T_0}{10}\right)} \tag{9a}$$

$$\xi_W = \frac{W}{W_0} \tag{9b}$$

where Q_{10} is an unknown parameter which is related to the respiration temperature sensitivity, T_0 and W_0 are the reference temperature and precipitation, which are set be to the maximum values of annual temperature and precipitation, respectively, across the study period. The two parameters, $\tau_E^{'}$ and Q_{10}, are calibrated by comparing the calculated $(\xi_T \xi_W)^{-1}\tau_E^{'}$ with the τ_E from model output, according to two indicators: the coefficient of determination (R^2) and the root mean square error (RMSE). The objective of the optimization method is to maximize R^2 and minimize RMSE:

$$Max\left(\frac{R^2}{RMSE}\right) \tag{10a}$$

$$R^2 = 1 - \frac{\sum_i [\tau_{E,i} - (\xi_{T,i}\xi_{W,i})^{-1}\tau_{E,i}']^2}{\sum_i (\tau_{E,i} - \overline{\tau_{E,i}})^2} \quad (10b)$$

$$RMSE = \sqrt{\frac{\sum_i (\tau_{E,i} - (\xi_{T,i}\xi_{W,i})^{-1}\tau_{E,i}')^2}{n}} \quad (10c)$$

where the subscript i refers to the time step, and n is the total time steps. In the optimization method, the parameters, τ_E' and Q_{10}, are obtained using the GRG non-linear solving method (Drud, 1985). For the optimization method for NPP, the two parameters, NPP' and Q_{10}, are calibrated using the same method as the carbon residence time.

2) Attribution analysis of carbon storage dynamics

After decomposing a complex land carbon cycle model into traceable components, we can better understand model output through attribution. Here we propose a variance decomposition method for the attribution analysis of carbon storage dynamics. This method is based on the covariance allocation principle for capital allocation, which is widely used for portfolio risk decomposition and attribution (Dhaene *et al.*, 2012). According to the covariance allocation principle, the variance of a variable can be decomposed into the sum of the covariances of its individual components and itself (see supporting information Text (S1)).

Three steps are taken to decompose the variance of terrestrial carbon storage into the contributions of the three variables, and the source factors. Following the transient traceability framework (Fig. 1), the variance of terrestrial carbon storage is firstly decomposed into the

contributions from carbon storage capacity and potential. The variance of carbon storage capacity is further decomposed into the contributions from carbon residence time and NPP. Finally, the variance of carbon residence time and NPP are decomposed into the contributions from the environmental scalars and the baseline values of them, respectively. To apply the variance decomposition method, the variable to be decomposed should be expressed as the sum of its components. Thus, we perform logarithmic transformation for the carbon storage capacity in equation (1), carbon residence time in equation (6), and NPP in equation (7) to separate them into several components, respectively. Details of the variance decomposition method for terrestrial carbon storage can be found in supporting information Text (S2).

c. The model inter-comparison projects

In this study, we compared the model output from the three MIPs, i.e., CMIP5, TRENDY-v1 and MsTMIP, based on the 3D model output space and the transient traceability framework. For the 3D model output space, carbon storage data (including carbon in the vegetation, soil, litter, and coarse woody debris pools), and NPP were obtained from the three MIPs. For each MIP, several models were selected based on the availability of model output in given historical simulations for our analysis (Table S1). In addition, outlier models, such as SiBCASA with unrealistically strong increase in carbon storage between two continuous years, were excluded.

In CMIP5, output from nine Earth System Models (ESMs) for the historical experiment covering a period from mid-nineteenth century to near present (1850 to 2005) were used. The ESMs allow us to explore the comprehensive behaviors of the Earth system through the coupling of ocean-atmosphere-land components. The land components of the ESMs differ in their

representations of vegetation types, soil properties, human disturbances, carbon and nitrogen pools, as well as their spatial resolutions (Anav et al. 2013). In addition, the nitrogen cycle is incorporated in BNU-ESM, CESM1-BGC and NorESM1-ME, and the latter two ESMs use the same land components as CLM4. The historical simulations are forced by changing conditions that are consistent with observations, including changes in atmospheric chemical composition and land use change (Taylor et al. 2012). Since the carbon storage and NPP output from ESMs in CMIP5 represent coupled simulations, the climate forcing used in our analysis was also obtained from the output of each ESM.

In TRENDY-v1, global simulations S2 (with historical climate, CO_2 fertilization) over the period 1901-2009 from nine Dynamic Global Vegetation Models (DGVMs) were used. The historical climate forcing data are taken from the combined data set of the climatology data produced by the Climate Research Unit (CRU) and the reanalysis data from National Centers for Environmental Prediction (NCEP)/National Center for Atmospheric Research (NCAR) (Harris et al. 2014; Kalnay et al. 1996). Annual resolution CO_2 data are sourced from historic atmospheric CO_2 from ice cores, and the National Oceanic and Atmospheric Administration (NOAA) for 1901-2009. Although the simulations S3 which use the historical land use change data from the History Database of the Global Environment (HYDE) (Hurtt et al. 2011), are more suitable for comparison with observations, the simulations S2 with a constant land-use mask were employed because the former simulations S3 are only available for a smaller subset of TRENDY models.

In MsTMIP, global simulations SG3 (with historical climate, CO_2 fertilization, land-use and land-cover change) from seven Terrestrial Biosphere Models (TBMs) were used. Four of the seven models are incorporated with nitrogen cycle, i.e., CLM4, CLM4VIC, ISAM and DLEM. The global simulations were run at 0.5° spatial resolution from 1901 to 2010 (Huntzinger et al.

337 2013). The standardized environmental driver data are described by Wei et al. (2014) in detail.
338 Similar to TRENDY-v1, the CRU-NCEP data set is also used as climate forcing in MsTMIP.
339 The atmospheric CO_2 concentration data for MsTMIP are prepared based on the GLOBVIEW-
340 CO_2 product, fossil fuel emissions, and CO_2 observations at Mauna Loa and the South Pole. The
341 land use and land cover change are prescribed by merging a statistic satellite-based land cover
342 product, with the time-varying land use harmonization data (Wei et al. 2014).

343 Air temperature and precipitation in the three MIPs were also used for traceability
344 analysis. We used the GCM driving forcing for individual models in CMIP5 and the CRU-NCEP
345 data for the models in TRENDY and MsTMIP. The monthly output from each model in the three
346 MIPs were processed following three steps. First, the components of all the carbon pools were
347 summed as terrestrial carbon storage. Second, monthly carbon storage, and NPP were aggregated
348 into annual totals for each grid cell, and then accumulated over all grid cells to calculate the
349 global annual values, respectively. Third, global mean precipitation and temperature over land
350 (excluding Antarctica and Greenland) for each year were similarly obtained from the monthly
351 data at each grid. The global annual data were finally used to derive the 3D model output space
352 and perform traceability analysis.

353

354 **3. Results**

355 *a. The 3D model output space*

356 Fig. 2a-c shows the distributions of annual carbon residence time, NPP, and carbon
357 storage potential for the models in CMIP5, MsTMIP and TRENDY at the global scale. The three
358 variables together determine the simulated annual carbon storage by the models in the 3D model

359 output space. Among the nine ESMs in CMIP5, NPP ranges from about 40 to 95 Pg C year^{-1}, and
360 the carbon residence time from about 20 to 55 years, while the carbon storage potential varies
361 from about -250 to 200 Pg C (Fig. 2a). The range of global mean annual carbon residence time is
362 generally small within each model, but annual NPP varies a lot for most models, with those that
363 include nitrogen limitation (i.e., BNU-ESM, CESM1-BGC and NorESM1-ME) showing smaller
364 mean values (43-44 Pg C year^{-1}) than other ESMs (60-80 Pg C year^{-1}) (Table S2). The carbon
365 storage capacity, i.e., the product of carbon residence time and NPP, ranges considerably from
366 less than 1200 Pg C for CESM1-BGC and NorESM1-ME to more than 3200 Pg C for MPI-
367 ESM-LR. For the seven TBMs in MsTMIP, the global annual carbon storage capacity also shows
368 large variation, which is attributed to the high variability in carbon residence time and NPP. In
369 addition, the carbon storage and carbon storage capacity are generally smaller for the four
370 models (i.e., CLM4, CLM4VIC, ISAM and DLEM) which incorporate a nitrogen cycle and
371 show lower mean annual NPP (38-51 Pg C year^{-1}) in comparison with other TBMs (50-73 Pg C
372 year^{-1}) (Table S2). However, the carbon residence time and NPP exhibit smaller variations across
373 the nine DGVMs in TRENDY, than those models in CMIP5 and MsTMIP, resulting in less
374 variation in the simulated carbon storage capacity (Fig. 2b and 2e).

375 The time series of global annual carbon storage and carbon storage capacity for the
376 models in CMIP5, MsTMIP and TRENDY are shown in Fig. 2d-f. Large diversity in the
377 simulated carbon storage is found for the 25 models. The annual carbon storage varies
378 considerably from less than 600 Pg C for CLM4VIC in MsTMIP to about 3200 PgC for MPI-
379 ESM-LR in CMIP5. The large range of carbon storage is highly related to that of the carbon
380 storage capacity. In responses to the external environmental changes, the carbon storage capacity
381 changes quickly, and it drives the carbon storage change. The change rate of annual carbon

382 storage is much slower than that of annual carbon storage capacity, as it is also regulated by the
383 internal carbon cycle processes.

384 The difference between carbon storage capacity and terrestrial carbon storage is
385 expressed as carbon storage potential in Fig. 2d-f. The inter-annual patterns of carbon storage in
386 the three MIPs are mainly affected by the carbon storage potential, because the sign and value of
387 the carbon storage potential determine the direction and rate of carbon storage change,
388 respectively. The nine DGVMs in TRENDY present positive carbon storage potential, with
389 larger values over the recent three decades than the first half of the 20th century, resulting in an
390 increasing direction of carbon storage change towards the carbon storage capacity. However, the
391 models in CMIP5 and MsTMIP exhibit lower variation in annual carbon storage. The carbon
392 storage potential fluctuates between positive and negative values, so the current carbon storage
393 rises and falls frequently within a small range over the study period. Several models in CMIP5
394 (i.e., CESM1-BGC, GFDL-ESM2G, MIROC-ESM and NorESM1-ME) and MsTMIP (i.e.,
395 CLM4, CLM4VIC, GTEC, ISAM and VEGAS2.1) show negative carbon storage potential over
396 most years, resulting in a long-term decline in carbon storage (Fig. 2d and 2f, Table S2).

397

398 *b. Traceability analyses of carbon residence time and NPP*

399 The carbon residence time and NPP are traced to their baseline values and the
400 environmental scalars. Fig. 3 shows the environmental space consisting of air temperature and
401 precipitation for the three MIPs. As the climate and carbon cycle form an intimately coupled
402 system, the environmental space of annual temperature and precipitation is different across the
403 nine ESMs in CMIP5. The simulated precipitation varies from about 680 to 1020 mm year^{-1}, and
404 temperature from 10.7 to 15.5 ^{o}C among the nine ESMs over the period 1850-2005 (Fig. 3).

405 Generally, the environmental space is not wide-spread for each model. The ranges of global
406 mean annual temperature and precipitation are less than 3 ^{o}C and 110 mm year^{-1}, respectively.
407 The environmental space is identical for the models in MsTMIP and TRENDY because the same
408 climate forcing (CRU-NCEP) are used to drive the uncoupled models. The global mean annual
409 precipitation and temperature over land (excluding Antarctica and Greenland) from CRU-NCEP
410 range from 718 to 818 mm year^{-1} and from 12.8 to 14.3 ^{o}C, respectively, over the period 1901-
411 2010 (Fig. 3). Because the traceability analysis is performed at the global annual scale, the
412 environmental space shows small diversity and does not reflect the seasonal and spatial
413 variability of temperature and precipitation, such as their large variations in semi-arid
414 ecosystems (Poulter et al. 2014).

415 Fig. 4 shows the dependence of carbon residence time and NPP on their baseline values
416 and the environmental scalars in the three MIPs. The difference in carbon residence time (or
417 NPP) results from the baseline carbon residence time (or baseline NPP) and the environmental
418 scalar across different models. There is a one- to three-fold variation in the baseline carbon
419 residence time and baseline NPP among the models in the three MIPs. The baseline carbon
420 residence time ranges from 21 to 42 years in CMIP5, from 23 to 35 years in TRENDY, and 12 to
421 37 years in MsTMIP (Table 2 and Fig. 4a-c). And the baseline NPP varies from 49 to 91 Pg C
422 year^{-1} in CMIP5, from 58 to 82 Pg C in TRENDY, and 42 to 85 Pg C year^{-1} in MsTMIP (Table 2
423 and Fig. 4d-f). However, the distributions of the environmental scalars are much closer across
424 different models, ranging from about 0.7 to 1, both for the carbon residence time and NPP. Thus,
425 the large range in carbon residence time and NPP in Fig. 2a-c is mainly attributed to the baseline
426 carbon residence time and baseline NPP among the models in the three MIPs.

It should be noted that the 3D points in Fig. 4 are scattered. In the traceability analysis, we use the optimization method to decompose the carbon residence time (or NPP) into the baseline carbon residence time (or baseline NPP) and the environmental scalar. As a consequence, the product of them cannot fully explain the variation in the carbon residence time (or NPP) (Table 2 and Fig. S2). The product of the baseline value and the environmental scalar explains 55±12% (mean ± 1 standard deviation) of the variation in the carbon residence time, and 59±16% of the variation in NPP, for the three MIPs. The optimization method performs better for the models in TRENDY (R^2=0.61±0.10 for carbon residence time and R^2=0.69±0.04 for NPP) and MsTMIP (R^2=0.58±0.10 for carbon residence time and R^2=0.66±0.07 for NPP). The variations in the carbon residence time and NPP are difficult to capture using the optimization method for several models in CMIP5, such as HadGEM2-ES, probably due to low or even opposite sensitivities of carbon residence time (and NPP) to temperature and precipitation over different regions. In addition, other environmental factors, such as atmospheric CO_2, land-use change and nitrogen availability, also influence the inter-annual variability of carbon residence time and NPP, which calls for an expanded parameterization that incorporates more controlling factors to improve the traceability analysis.

c. Variance decomposition of the simulated carbon storage

The variation in the carbon storage is decomposed into several components for the three MIPs using the variance decomposition method (Fig. 5). The carbon storage variation is dominated by the carbon residence time and NPP, and the absolute contribution of the carbon storage potential is less than 1%. The baseline carbon residence time and baseline NPP contribute more than 90% to the variation in carbon residence time and NPP, respectively, for

each MIP and all three MIPs combined. Specifically, the contribution of the baseline carbon residence time to the carbon storage variation is 45% for CMIP5, 46% for TRENDY, 68% for MsTMIP, and 44% for the three MIPs, and that of the baseline NPP is 50% for CMIP5, 48% for TRENDY, 34% for MsTMIP, and 55% for the three MIPs. However, the temperature and water scalars contribute no more than 5% of variations in the carbon residence time and NPP, respectively. As a consequence, the variation in carbon storage is dominated by the baseline carbon residence time and baseline NPP. These results are consistent with the large ranges of the baseline carbon residence time and baseline NPP, and the close distributions of the environmental scalars across different models (Fig. 4).

Although carbon storage variation is mainly attributed to baseline carbon residence and baseline NPP among different models, it is determined by the environmental conditions for individual models when the baseline values are constant. Fig. 6 shows the distributions of the air temperature contributions to the variations in carbon residence time and NPP for all three MIPs. Within each model, the total contribution of the temperature and water scalars to the variations in carbon residence time and NPP equals 100%, according to the traceability framework. The contributions of precipitation are shown in Fig. S3. In CMIP5, air temperature explains most of the variations in the carbon residence time (74±20%) and NPP (63±21%) for the nine ESMs. The contributions of air temperature in TRENDY (40±13% to carbon residence time and 63±15% to NPP) and MsTMIP (59±13% to carbon residence time and 49±18% to NPP) are smaller than those in CMIP5. For the 25 models in the three MIPs, the mean contribution of air temperature is more than precipitation, both for the carbon residence time (58±22%) and NPP (59±19%).

4. Discussion

a. Model differences in the baseline carbon residence time and baseline NPP

All the models in the three MIPs can simulate the processes of photosynthetic carbon input, carbon allocation and transformation, and carbon loss through respiration. Most terrestrial carbon cycle models broadly share a similar structure for carbon cycle simulation, i.e., a pool-and-flux structure (Luo et al. 2015). In these models, the processes of carbon flow through different pools from its entrance via photosynthesis to its release via respiration are simulated based on a set of carbon balance equations. As indicated by Luo et al. (2015), the internal carbon cycle processes can be characterized by five fundamental properties for all terrestrial ecosystems: compartmentalization, photosynthesis as the dominant carbon input, partitioning among pools, donor pool-dominant transfers, and first-order decay. These five properties have been incorporated into terrestrial carbon cycle models using the carbon balance equations, which can be further summarized as a matrix equation. For a given carbon cycle model, its structure can be represented by the matrix equation, with a given number of carbon balance equations. Despite the fact that model structures show a high degree of underlying similarity, across-model variation in carbon cycle parameters results in large differences in NPP and carbon residence time.

Photosynthetic carbon assimilation is the major pathway of carbon flow in terrestrial ecosystems, and it is usually simulated based on the Farquhar model. In the Farquhar model, assimilation rate is jointly controlled by the rubisco limitation of carboxylation and the electron transport rate (Farquhar et al. 1980). Leaf photosynthetic capacity, as determined by rubisco and electron transport capacities, plays an important role in the simulation of ecosystem carbon input. In addition, ecosystem carbon input (e.g., NPP) is also affected by leaf area index, and regulated by environmental factors, such as temperature, radiation and water availability (Boisvenue;

Running 2006; Nemani et al. 2003; Schloss et al. 1999). In this study, NPP variation is traced to the baseline NPP and two environmental scalars. Baseline NPP is related to the maximum carbon input at optimal environmental conditions, and the environmental scalars represent the environmental limitations.

Once assimilated, photosynthetic carbon is allocated into different plant pools, e.g., leaves, stems and roots, for plant biomass growth and plant respiration. After death, plant organs are transferred to litter pools, which will be decomposed by microorganisms through heterotrophic respiration, or transferred to the soil pool in the form of soil organic matter. Soil organic carbon can be stored for hundreds to thousands of years before it is released back into the atmosphere through microbial respiration (Luo and Zhou, 2006). The carbon decomposition rate (i.e., the inverse of carbon residence time) in terrestrial ecosystems is greatly affected by environmental conditions, especially temperature and soil moisture (Davidson; Janssens 2006; Sierra et al. 2015). The maximum rate of carbon decomposition at optimal temperature and moisture conditions corresponds to the baseline carbon residence time, i.e., the shortest carbon residence time.

In this study, the processes of carbon input and output simulated in the terrestrial carbon cycle models are summarized as ecosystem NPP and carbon residence time, respectively. The carbon cycle parameters, especially those which determine carbon uptake and release at optimal environmental conditions, are important for simulations of NPP and carbon residence time as they alter their corresponding baseline values. Thus, the differences in the carbon cycle parameters can be measured by the variations of the baseline NPP and baseline carbon residence time. By comparing the output of the Australian Community Atmosphere Biosphere Land Exchange (CABLE) model and Community Land Model version 3.5 (CLM3.5 or CLM-CASA'),

Rafique et al. (2016) indicated that the parameter setting related to NPP and the baseline carbon residence time leads to the eventual model differences. Friend et al. (2014) also identified variations in the carbon residence time as the key difference among models to explain their diverging projections. Our study is consistent in showing that the baseline NPP and baseline carbon residence time contribute to more than 90% to the carbon storage variation, much more than the external environmental scalars or forcing. This result confirms the important role of model parameters which affect the baseline carbon residence time and baseline NPP in determining the output of terrestrial carbon cycle models. For future model improvement, modelers should pay more attention to the carbon cycle processes and parameters related to the baseline carbon residence time and baseline NPP.

b. Model inter-comparison across the three MIPs

Different from previous model inter-comparison studies (Keenan et al. 2012; Schwalm et al. 2010; Sitch et al. 2008; Zaehle et al. 2014), which aim to compare and improve model performance through model-data analysis, this study attributes the large variations in annual carbon storage to the variations in carbon residence time, NPP, and carbon storage potential to understand inter-model differences.

The 25 models in the three MIPs are different in terms of the three decomposed parameters, resulting in great spreads in annual carbon storage. The CMIP5 and MsTMIP present large variations in the simulated carbon storage among different models than TRENDY. According to the variance decomposition method, the wide-spread baseline carbon residence time and baseline NPP result in large carbon storage variation in CMIP5 and MsTMIP. The large variations in the carbon residence time and NPP among different models may be related to land-

use change (Erb et al. 2016), since the simulations in CMIP5 and MsTMIP employed time-variant historical land-use change with different representations of vegetation types, while TRENDY models utilized a constant land-use mask. This is reflected by the nine DGVMs in TRENDY, which consistently show an increasing trend of carbon storage (capacity) over the period 1901-2010, especially the recent three decades. On the contrary, there is no obvious trends in CMIP5 and MsTMIP simulations, where the CO_2 fertilization effect on carbon storage (capacity) may be attenuated by land-use change. The increasing trend of carbon storage in TRENDY is implied by the large and mostly positive carbon storage potential, which determines the direction and rate of carbon storage change (see also Fig. 2b). However, the effects of land-use change on carbon residence time and NPP were not incorporated in the transient traceability analysis in this study. Nevertheless, land use changes and other disturbances influence the carbon cycle by: (i) either depleting or adding carbon in pools; (ii) either decreasing or increasing canopy photosynthesis; and (iii) altering carbon residence times via changes in respiration and decomposition (Luo and Weng, 2011). All those influences induced by land use changes can be represented by the three dynamics properties (i.e., carbon input, residence time, and the carbon storage potential) and thus analyzed by those techniques developed in this study. The carbon cycle is coupled with the climate dynamics for the nine ESMs in CMIP5 but not for the models in TRENDY and MsTMIP. The nine ESMs allow feedback between carbon cycling and climate change, while the climate forcing is prescribed in TRENDY and MsTMIP. The traceability analysis shows that the dependence of the carbon residence time and NPP on the environmental scalars is stronger for the uncoupled models than that for the coupled models (Fig. 4). The relationships between the carbon residence time (or NPP) and the environmental variables are more complex in the ESMs, given the feedbacks of carbon cycle and climate change (Heimann;

564 Reichstein 2008; Sokolov et al. 2008). Thus, the variations in the carbon residence time and NPP
565 are not easy to be captured by the temperature and water scalars.

566 Although the environmental space varies with the simulated climate for the models in
567 CMIP5, and is identical in TRENDY and MsTMIP, the total contribution of the environmental
568 scalars to the carbon storage variation in CMIP5 is no more than that in TRENDY and MsTMIP.
569 Indeed, both the carbon residence time and NPP are climate dependent. By comparing the
570 "coupled" and "uncoupled" simulations of 11 coupled climate-carbon cycle models,
571 Friedlingstein et al. (2006) show that the impact of climate change on land carbon storage is
572 significant in all models. However, the climate impact on the carbon storage variation across
573 different models is weak, both for the coupled and uncoupled models, because they strongly
574 differ in model parameters of carbon cycle processes. Our results indicate that the difference in
575 the environmental scalars is much smaller than that in the baseline carbon residence time and
576 baseline NPP among the models in all of the three MIPs.

577 Compared with precipitation, air temperature contributes more to the variations in carbon
578 residence time and NPP for the 25 models. Many studies have shown that carbon cycle
579 processes, including carbon accumulation and decomposition, are sensitive to climate warming
580 (Lu et al. 2013; Xia et al. 2014). However, the change in precipitation varies greatly over
581 different regions, resulting in inconsistent effects on the carbon cycle across the globe, so the
582 precipitation impact on terrestrial carbon sequestration is rather weak at the global scale
583 (Sokolov et al. 2008). The models in CMIP5 exhibit larger mean temperature contribution than
584 those in TRENDY and MsTMIP. The large temperature contribution for the nine ESMs may be
585 related to the strong positive feedback between carbon cycle and climate warming (Luo 2007;
586 Zeng 2004), which further enhances the role of air temperature in the carbon cycle processes.

It should be noted that differences in model behaviors are also related to whether a nitrogen cycle is included in the model. Since the productivity of many terrestrial ecosystems is limited by lack of reactive nitrogen (Norby et al. 2010; Zhang et al. 2014), and the CO_2 fertilization effect is strongly down regulated by nitrogen limitation (Rastetter et al. 1992; Hungate et al. 2003; Walker et al. 2015), NPP is generally lower in the models with nitrogen limitation than those that do not include nitrogen limitation, resulting in smaller carbon storage capacity and carbon storage. We found the carbon storage potential is mostly negative for the models that include a nitrogen limitation, which indicates a decreasing trend of carbon storage over the study period, while the other models exhibit positive carbon storage potential over most years. It was reported that nitrogen limitation will reduce the CO_2 fertilization effect, and even cause a reduced NPP for some ecosystems (McMurtrie et al. 2008; Norby et al. 2010; Thornton et al. 2007). The differing behavior between models with and without a nitrogen cycle indicates that the carbon-nitrogen feedback should be considered when assessing model differences.

c. Understanding the variation in carbon storage among different models

In this study, we developed a suite of new techniques for tracing predominant model parameters that govern the simulated global carbon budget in a multi-model setting. We applied these methods to compare the carbon storage dynamics simulated by 25 models in three MIPs. These new techniques include a 3D model outputs space, a transient traceability framework, and a variance decomposition method, which allow us to elucidate the main source of variability in the historical simulations of carbon storage across different models. In addition, these new techniques can be also applied to future projections to understand large divergence in model predictions (Friedlingstein et al. 2014).

610 The 3D model output space can measure the difference in the projected carbon storage
611 dynamics in terms of NPP, carbon residence time, and carbon storage potential (Fig. 2, Luo et al.
612 (2017)). Despite differences in model structure and carbon cycle parameters, the differences in
613 photosynthetic processes and parameter values can be summarized by that in NPP. Similarly, the
614 differences in processes after photosynthesis and relevant parameters are revealed by the
615 variation in the carbon residence time across the different models. The product of NPP and
616 carbon residence time measures the difference in carbon storage capacity at steady state, and the
617 carbon storage potential can capture the transient dynamics of the terrestrial carbon cycle in
618 response to the changes in environmental conditions. The 3D model output space can clearly
619 illustrate how and how much the model output differ. Thus, we can perform model evaluations
620 by comparing model output with observations in terms of the three variables, and improve model
621 projections by adjusting the parameters related to NPP and carbon residence time according to
622 their differences with observed values.

623 The transient traceability framework can decompose a complex carbon cycle model into
624 traceable components by simulating biogeochemical processes. It extended the traceability
625 framework developed by Xia et al. (2013) in two aspects. First, this new framework can directly
626 analyze the transient dynamics of terrestrial carbon storage simulated by the models through
627 involving the third dimension: the carbon storage potential. Second, the modeled NPP is
628 decomposed into the baseline NPP and environmental scalars for temperature and precipitation.
629 Thus, we can attribute the model differences in NPP and carbon residence time to the variability
630 in model parameters and environmental forcing.

631 The variance decomposition method can separate the relative contributions of NPP,
632 carbon residence time and carbon storage potential to variations in terrestrial carbon storage.

633 Thus, the variation in the simulated carbon storage among different models can be quantitatively
634 attributed to the three variables and hence the source factors. In addition, our decomposition
635 method is also applicable to assess the responses of carbon storage to the changing environment
636 (e.g., climate warming, rising atmosphere CO_2, and other disturbances), and quantify the
637 contributions of the decomposed components to the projected change in carbon storage. This
638 quantitative method can help us to investigate the response mechanisms of the terrestrial carbon
639 storage to the environmental changes and therefore better predict terrestrial carbon sequestration
640 response under future climate change.

641

642 *d. Limitations and recommendations*

643 In this study, we compared the simulated global mean carbon storage dynamics in the
644 three MIPs based on the 3D model output space, identified the sources of carbon storage
645 variation following the traceability framework, and quantified the relative contributions of the
646 source factors. The three MIPs show a large spread in simulated carbon storage dynamics, which
647 is effectively revealed by the 3D model output space. Specifically, our study shows that the
648 baseline NPP and carbon residence time are major sources of inter-model variations. Future
649 modelling research needs to better constrain the two parameters with observations almost all
650 carbon-related variables, including plant allocation, decomposition, microbial carbon use
651 efficiency, especially under favorable environmental conditions in order to improve the model
652 projections.

653 Our study is the first to perform model inter-comparison based on the 3D model output
654 space and the transient traceability framework in a multi-MIP setting. This is a post-simulation
655 model evaluation. We took the terrestrial ecosystem as one pool to estimate the carbon residence

time and carbon storage potential while the original models have complex structures and variable parameters. Using this simple yet effective method, we are able to obtain the three variables and environmental scalars of the models to develop the 3D model output space, perform traceability analysis, and conduct variance decomposition for understanding model variations. These post-MIP analyses demonstrate that the three techniques developed in this study can be used as an important means to track the origins of model differences from a completed MIP. The main limitation of this study is that the model inter-comparison analyses were performed at the global annual scale. The motivation of this is to get an overview on inter-model differences in simulating land carbon storage. More studies should be done in the future to gain understanding of the sub-annual and grid-scale variability of the three variables, and the difference among biomes as well. Another limitation is that the traceability analysis of carbon residence time and NPP was done by only considering the effect of temperature and precipitation. Although the optimization method explained most of the variations in carbon residence time and NPP for the majority of the models, we need more information on regulations of carbon cycle processes by various factors and processes from original models to fully understand variations in model performance. Should we have all carbon balance equations, response functions, and their parameters, the transient traceability analysis can account for almost all variations among models (Luo et al. 2017). For future MIPs, we recommend a matrix approach to reorganize all carbon balance equations in any original model into one matrix equation as for CLM4.5 (Huang et al., 2017). The matrix approach is applicable to almost all land carbon cycle models. Once all the models that are involved in one MIP are converted to matrix equations, we can analyze model uncertainty in a unified diagnostic system. That is, all the land carbon cycle models are represented with one unified formula; model outputs are evaluated in the 3D space; and

679 uncertainty among models can be traced to various components (e.g., carbon input, plant
680 allocation, decomposition rates, and environmental scalars). We expect that this diagnostic
681 system can greatly improve our understanding of uncertainty sources of land carbon modeling.
682 So, those techniques developed in this study, which are parts of the diagnostic system, can
683 effectively identify the sources of model differences and guide directions for future model
684 improvement.

685 Future research is needed to perform the analysis at the grid or regional scale. The global
686 analysis cannot fully reveal the origins of differences in model output, and may introduce some
687 biases (e.g., due to compensatory effects in time and/or space) in the relationship between the
688 carbon residence time (or NPP) and the environmental scalars. At the regional scale, the
689 decomposed traceable components can be compared with observations to illustrate the deviations
690 of model output from real-world values. In addition, we can determine the key processes or
691 parameters that explain the differences among models as well as between models and
692 observations over different regions. For regional analysis, more environmental factors should be
693 considered in the traceability analysis, such as solar radiation, atmospheric CO_2, land-use change
694 and nitrogen availability, to capture the temporal and spatial variability of the carbon residence
695 time and NPP. The carbon storage potential should also be decomposed into its traceable
696 components to further enhance our understanding. As indicated in equation (2), the carbon
697 storage potential can be decomposed into the chasing time and the rate of carbon storage change.
698 The chasing time is closely related to the carbon residence time, and they are identical when we
699 use the one-pool model. The rate of carbon storage change is affected by various factors, both
700 internal processes and external forcing. So it is critical to perform decomposition analysis to
701 identify key processes governing the rate of carbon storage change. Through analyzing the

carbon storage potential, our transient traceability framework can better evaluate the transient terrestrial carbon cycle responses to external forcing and internal processes. Upon careful consideration of the carbon cycling processes, their responses to environmental drivers, and model parameters, the transient traceability framework can elucidate how various processes and parameter settings influence ecosystem carbon storage through the simulated changes in NPP, carbon residence time and carbon storage potential. Thus, we can efficiently improve model performance towards more realistic projections by adjusting the highlighted carbon cycle processes and parameters in future studies.

Acknowledgements We acknowledge the World Climate Research Programme's Working Group on Coupled Modelling, which is responsible for CMIP, and we thank the climate modeling groups (listed in Table S1) for producing and making available their model output. For CMIP the U.S. Department of Energy's Program for Climate Model Diagnosis and Intercomparison provides coordinating support and led development of software infrastructure in partnership with the Global Organization for Earth System Science Portals. Funding for the Multi-scale synthesis and Terrestrial Model Intercomparison Project (MsTMIP; http://nacp.ornl.gov/MsTMIP.shtm) activity was provided through NASA ROSES Grant NNX10AG01A. Data management support for preparing, documenting, and distributing model driver and output data was performed by the Modeling and Synthesis Thematic Data Center at Oak Ridge National Laboratory (ORNL; http://nacp.ornl.gov), with funding thorough NASA ROSES Grant NNH10AN681. Finalized MsTMIP data products are archived at the ORNL DAAC (http://daac.ornl.gov). We acknowledge the TRENDY-v1 modelers, including Benjamin Poulter from Montana State University, for contributing model output used in this

work. This paper is financially supported by the Research and Development Special Fund for Public Welfare Industry of the Ministry of Water Research in China (No. 201501028). JBF and CRS were supported in part by NASA's Carbon Cycle Science program. JBF was also supported in part by NASA's Terrestrial Ecology and Carbon Monitoring System programs. JT acknowledges RCN funded project EVA (229771) and BCCR-BIGCHANGE.

REFERENCES

Anav, A., G. Murray-Tortarolo, P. Friedlingstein, S. Sitch, S. Piao, and Z. Zhu, 2013: Evaluation of Land Surface Models in Reproducing Satellite Derived Leaf Area Index over the High-Latitude Northern Hemisphere. Part II: Earth System Models. *Remote Sens.*, **5,** 3637-3661.

Ahlström, A., G. Schurgers, A. Arneth, and B. Smith, 2012: Robustness and uncertainty in terrestrial ecosystem carbon response to CMIP5 climate change projections. *Environ. Res. Lett.*, **7**(4), 044008.

Boisvenue, C., and S. W. Running, 2006: Impacts of climate change on natural forest productivity - evidence since the middle of the 20th century. *Global Change Biol.*, **12,** 862-882.

Cramer, W., and Coauthors, 1999: Comparing global models of terrestrial net primary productivity (NPP): overview and key results. *Global Change Biol.*, **5,** 1-15.

De Kauwe, M. G., and Coauthors, 2014: Where does the carbon go? A model-data intercomparison of vegetation carbon allocation and turnover processes at two temperate forest free-air CO_2 enrichment sites. *New Phytol.*, **203,** 883-899.

Davidson, E. A., and I. A. Janssens, 2006: Temperature sensitivity of soil carbon decomposition and feedbacks to climate change. *Nature*, **440,** 165-173.

748 Drud, A., 1985:CONOPT: A GRG code for large sparse dynamic nonlinear optimization
749 problems. *Math. Program.*, **31**, 153-191.Erb, K. H., and Coauthors, 2016: Biomass turnover
750 time in terrestrial ecosystems halved by land use. *Nat. Geosci*, **9,** 674-678.
751 Exbrayat, J. F., A. J. Pitman, and G. Abramowitz, 2014: Response of microbial decomposition to
752 spin-up explains CMIP5 soil carbon range until 2100, *Geosci. Model Dev.*, **7,** 2683-2692.
753 Farquhar, G. D., S. von Caemmerer, and J. Berry, 1980: A biochemical model of photosynthetic
754 CO_2 assimilation in leaves of C3 species. *Planta*, **149,** 78-90.
755 Fisher, J. B., D. N. Huntzinger, C. R. Schwalm, and S. Sitch, 2014: Modeling the Terrestrial
756 Biosphere. *Annu. Rev. Environ. Resour.*, **39,** 91-123.
757 Friedlingstein, P., and Coauthors, 2006: Climate-carbon cycle feedback analysis: Results from
758 the C^4MIP model intercomparison. *J. Climate*, **19,** 3337-3353.
759 Friedlingstein, P., and Coauthors, 2014: Uncertainties in CMIP5 Climate Projections due to
760 Carbon Cycle Feedbacks. *J. Climate*, **27,** 511-526.Friend, A. D., and Coauthors, 2014:
761 Carbon residence time dominates uncertainty in terrestrial vegetation responses to future
762 climate and atmospheric CO_2. *Proc. Natl. Acad. Sci. USA*, **111,** 3280-3285.
763 Friend, A.D., A. K., Stevens, R. G., Knox, and M. G. R., Cannell, 1997: A process-based,
764 terrestrial biosphere model of ecosystem dynamics (Hybrid v3. 0). *Ecol. Model.*, **95**, 249-
765 287.
766 Harris, I., P. D. Jones, T. J. Osborn, and D. H. Lister, 2014: Updated high-resolution grids of
767 monthly climatic observations - the CRU TS3.10 Dataset. *Int. J. Climatol.*, **34,** 623-642.
768 Heimann, M., and M. Reichstein, 2008: Terrestrial ecosystem carbon dynamics and climate
769 feedbacks. *Nature*, **451,** 289-292.

770 Huang, Y., and Coauthors, 2017: Matrix approach to land carbon cycle modeling: A case study
771 with Community Land Model. *Global Change Biol.*.
772 Hungate, B. A., J. S. Dukes, M. R. Shaw, Y. Luo, and C. B. Field, 2003: Atmospheric science.
773 Nitrogen and climate change. *Science*, **302,** 1512-1513.
774 Huntzinger, D. N., and Coauthors, 2013: The North American Carbon Program Multi-Scale
775 Synthesis and Terrestrial Model Intercomparison Project - Part 1: Overview and
776 experimental design. *Geosci. Model Dev.*, **6,** 2121-2133.
777 Hurtt, G. C., and Coauthors, 2011: Harmonization of land-use scenarios for the period 1500–
778 2100: 600 years of global gridded annual land-use transitions, wood harvest, and resulting
779 secondary lands. *Climatic Change*, **109,** 117-161.
780 Ichii, K., and Coauthors, 2010: Multi-model analysis of terrestrial carbon cycles in Japan:
781 limitations and implications of model calibration using eddy flux observations.
782 *Biogeosciences*, **7,** 2061-2080.
783 Kalnay, E., M. Kanamitsu, R. Kistler, M. Collins, D. Deaven, and e. al., 1996: The NCEP/NCAR
784 40-year reanalysis project. *Bull. Amer. Meteor. Soc.*, **77,** 437-471.
785 Keenan, T. F., and Coauthors, 2012: Terrestrial biosphere model performance for inter-annual
786 variability of land-atmosphere CO_2 exchange. *Global Change Biol.*, **18,** 1971-1987.
787 Knutti, R., and J. Sedláček, 2012: Robustness and uncertainties in the new CMIP5 climate model
788 projections. *Nat. Climate Change*, **3,** 369-373.
789 Lu, M., and Coauthors, 2013: Responses of ecosystem carbon cycle to experimental warming: A
790 meta analysis. *Ecology*, **94,** 726-738.
791 Luo, Y., 2007: Terrestrial Carbon-Cycle Feedback to Climate Warming. *Annu. Rev. Ecol. Evol.*
792 *Syst.*, **38,** 683-712.

793 Luo, Y., and E. Weng, 2011: Dynamic disequilibrium of the terrestrial carbon cycle under global
794 change. *Trends Ecol. Evol.*, 26, 96-104.
795 Luo, Y., T. F. Keenan, and M. Smith, 2015: Predictability of the terrestrial carbon cycle. *Global*
796 *Change Biol.*, **21,** 1737-1751.
797 Luo, Y., and Coauthors, 2003: Sustainability of terrestrial carbon sequestration: A case study in
798 Duke Forest with inversion approach. *Global Biogeochem. Cycles*, **17,** 1021,
799 doi:1010.1029/2002GB001923.
800 Luo, Y., and Coauthors, 2017: Transient dynamics of terrestrial carbon storage: mathematical
801 foundation and its applications. *Biogeosciences*, **14,** 145-161.
802 McMurtrie, R. E., R. J. Norby, B. E. Medlyn, R. C. Dewar, D. A. Pepper, P. B. Reich, and C. V.
803 Barton, 2008: Why is plant-growth response to elevated CO_2 amplified when water is
804 limiting, but reduced when nitrogen is limiting? A growth-optimisation hypothesis. *Funct.*
805 *Plant Biol.*, **35,** 521-534.
806 Meehl, G. A., C. Covey, B. McAvaney, M. Latif, and R. J. Stouffer, 2005: Overview of the
807 Coupled Model Intercomparison Project. *Bull. Amer. Meteor. Soc.*, **86,** 89-93.
808 Nishina, K., and Coauthors, 2014: Quantifying uncertainties in soil carbon responses to changes
809 in global mean temperature and precipitation, *Earth Syst. Dynam.*, **5,** 197-209.
810 Nishina, K., and Coauthors, 2015: Decomposing uncertainties in the future terrestrial carbon
811 budget associated with emission scenarios, climate projections, and ecosystem simulations
812 using the ISI-MIP results, *Earth Syst. Dynam.*, **6,** 435-445.
813 Nemani, R. R., and Coauthors, 2003: Climate-driven increases in global terrestrial net primary
814 production from 1982 to 1999. *Science*, **300,** 1560-1563.

Norby, R. J., J. M. Warren, C. M. Iversen, B. E. Medlyn, and R. E. McMurtrie, 2010: CO_2 enhancement of forest productivity constrained by limited nitrogen availability. *Proc. Natl. Acad. Sci. USA*, **107,** 19368-19373.

Oleson, K., and Coauthors (2013) Technical description of version 4.5 of the Community Land Model (CLM). In *NCAR Technical Note NCAR/TN-503+STR*. National Center for Atmospheric Research, Boulder, CO, USA.

Parton, W. J. (1996). The CENTURY model. In *Evaluation of soil organic matter models* (pp. 283-291). Springer Berlin Heidelberg.

Potter, C. S., J. T. Randerson, C. B. Field, P. A. Matson, P. M. Vitousek, H. A. Mooney, and S. A. Klooster, 1993: Terrestrial ecosystem production: a process model based on global satellite and surface data. *Global Biogeochem. Cycles*, **7,** 811-841.

Rafique, R., J. Xia, O. Hararuk, G. R. Asrar, G. Leng, Y. Wang, and Y. Luo, 2016: Divergent predictions of carbon storage between two global land models: attribution of the causes through traceability analysis. *Earth Syst. Dynam.*, **7,** 649-658.

Rastetter, E., R. McKane, G. Shaver, and J. Melillo, 1992: Changes in C storage by terrestrial ecosystems: how C-N interactions restrict responses to CO_2 and temperature. *Water, Air, & Soil Pollution*, **64,** 327-344.

Running, S. W., E. R., Hunt, 1993: Generalization of a forest ecosystem process model for other biomes, BIOME-BCG, and an application for global-scale models. Scaling processes between leaf and landscape levels. In: *Scaling Physiological Processes: Leaf to Globe* (Ehleringer JR, Field CB, eds.), pp. 141-158. Academic Press, San Diego.

836 Schloss, A. L., D. W. Kicklighter, J. Kaduk, U. Wittenberg, and Coauthors, 1999: Comparing
837 global models of terrestrial net primary productivity (NPP): comparison of NPP to climate
838 and the Normalized Difference Vegetation Index (NDVI). *Global Change Biol.*, **5,** 25-34.
839 Schwalm, C. R., and Coauthors, 2010: A model-data intercomparison of CO_2 exchange across
840 North America: Results from the North American Carbon Program site synthesis. *J.*
841 *Geophys. Res.*, **115,** G00H05
842 Sierra, C. A., S. E. Trumbore, E. A. Davidson, S. Vicca, and I. Janssens, 2015: Sensitivity of
843 decomposition rates of soil organic matter with respect to simultaneous changes in
844 temperature and moisture. *J. Adv. Model. Earth Syst.*, **7,** 335-356.
845 Sitch, S., and Coauthors, 2008: Evaluation of the terrestrial carbon cycle, future plant geography
846 and climate-carbon cycle feedbacks using five Dynamic Global Vegetation Models
847 (DGVMs). *Global Change Biol.*, **14,** 2015-2039.
848 Sitch, S., and Coauthors, 2015: Recent trends and drivers of regional sources and sinks of carbon
849 dioxide. *Biogeosciences*, **12,** 653-679.
850 Sokolov, A. P., D. W. Kicklighter, J. M. Melillo, B. S. Felzer, C. A. Schlosser, and T. W.
851 Cronin, 2008: Consequences of Considering Carbon–Nitrogen Interactions on the Feedbacks
852 between Climate and the Terrestrial Carbon Cycle. *J. Climate*, **21,** 3776-3796.
853 Taylor, K. E., R. J. Stouffer, and G. A. Meehl, 2012: An Overview of CMIP5 and the
854 Experiment Design. *Bull. Amer. Meteor. Soc.*, **93,** 485-498.
855 Thornton, P. E., J.-F. Lamarque, N. A. Rosenbloom, and N. M. Mahowald, 2007: Influence of
856 carbon-nitrogen cycle coupling on land model response to CO_2 fertilization and climate
857 variability. *Global Biogeochem. Cycles*, **21,** GB4018.

858 Todd-Brown, K. E. O., J. T. Randerson, W. M. Post, F. M. Hoffman, C. Tarnocai, E. A. G.
859 Schuur, and S. D. Allison, 2013: Causes of variation in soil carbon simulations from CMIP5
860 Earth system models and comparison with observations. *Biogeosciences*, **10,** 1717-1736.
861 Walker, A. P., and Coauthors, 2015: Predicting long-term carbon sequestration in response to
862 CO_2 enrichment: How and why do current ecosystem models differ? *Global Biogeochem.*
863 *Cycles*, **29,** 476-495.
864 Wei, Y., and Coauthors, 2014: The North American Carbon Program Multi-scale Synthesis and
865 Terrestrial Model Intercomparison Project - Part 2: Environmental driver data. *Geosci.*
866 *Model Dev.*, **7,** 2875-2893.
867 Woodward, F. I., T. M. Smith, and W. R. Emanuel, 1995: A global land primary productivity
868 and phytogeography model. *Global Biogeochem. Cycles*, **9,** 471-490.
869 Xia, J., Y. Luo, Y. P. Wang, and O. Hararuk, 2013: Traceable components of terrestrial carbon
870 storage capacity in biogeochemical models. *Global Change Biol.*, **19,** 2104-2116.
871 Xia, J., J. Q. Chen, S. L. Piao, P. Ciais, Y. Q. Luo, and S. Q. Wan, 2014: Terrestrial carbon cycle
872 affected by non-uniform climate warming. *Nat. Geosci.*, **7,** 173-180.
873 Zaehle, S., and Coauthors, 2014: Evaluation of 11 terrestrial carbon-nitrogen cycle models
874 against observations from two temperate Free-Air CO_2 Enrichment studies. *New Phytol.*,
875 **202,** 803-822.
876 Zeng, N., 2004: How strong is carbon cycle-climate feedback under global warming? *Geophys.*
877 *Res. Lett.*, **31,** L20203.
878 Zhang, Q., Y. P. Wang, R. J. Matear, A. J. Pitman, and Y. J. Dai, 2014: Nitrogen and
879 phosphorous limitations significantly reduce future allowable CO_2 emissions. *Geophys. Res.*
880 *Lett.*, **41,** 632-637.

881

882 TABLE 1. Symbols and parameters used in this study.

Symbol or parameter	Definition	Unit
X	Carbon storage	Pg C
X_c	Carbon storage capacity	Pg C
X_p	Carbon storage potential	Pg C
$X^{'}$	Rate of carbon storage change	Pg C year^{-1}
NPP	Net primary productivity	Pg C year^{-1}
τ_E	Carbon residence time	year
τ_{ch}	Chasing time	year
ξ	Environmental scalar for carbon residence time	-
δ	Environmental scalar for NPP	-
$\tau_E^{'}$	Baseline carbon residence time	year
$NPP^{'}$	Baseline NPP	Pg C year^{-1}
ξ_T	Temperature scalar for carbon residence time	-
ξ_W	Water scalar for carbon residence time	-
δ_T	Temperature scalar for NPP	-
δ_W	Water scalar for NPP	-
Q_{10}	Respiration temperature sensitivity	-
T_0	Reference temperature	℃
T	Mean annual temperature	℃
W_0	Reference precipitation	mm year^{-1}
W	Annual total precipitation	mm year^{-1}

883

884 TABLE 2. Calibrated parameters and the performance of the optimization method for the carbon
885 residence time and NPP. T_0 and W_0 are the reference values of temperature and precipitation.

	Models	T_0 (°C)	W_0 (mm year^{-1})	The carbon residence time				NPP			
				$\tau_E{}'$ (year)	Q_{10}	R^2	$RMSE$	NPP' (P g C year^{-1})	Q_{10}	R^2	$RMSE$
CMIP5	BNU-ESM	14.05	1022.75	32.31	1.64	0.53	1.06	52.69	2.51	0.60	1.76
	CanESM2	15.45	769.63	28.34	2.45	0.46	1.21	69.27	1.75	0.31	2.69
	CESM1-BGC	14.34	984.43	21.84	2.41	0.61	0.85	48.77	1.68	0.61	0.95
	GFDL-ESM2G	13.78	956.57	23.69	4.81	0.35	1.91	81.24	2.39	0.31	3.97
	HadGEM2-ES	13.43	893.66	24.37	0.74	0.34	2.12	64.01	0.67	0.25	5.86
	IPSL-CM5B-LR	13.30	761.16	22.63	2.52	0.62	0.92	80.07	3.33	0.64	2.89
	MIROC-ESM	14.77	956.47	42.38	2.59	0.45	1.26	65.61	1.51	0.23	1.44
	MPI-ESM-LR	13.94	803.91	37.31	2.07	0.62	1.36	91.11	2.22	0.59	3.21
	NorESM1-ME	13.41	940.70	20.83	3.42	0.36	1.01	50.63	2.11	0.35	1.22
TRENDY	CLM4C	14.31	817.81	28.02	1.36	0.46	0.61	77.66	2.58	0.67	2.05
	CLM4CN	14.31	817.81	26.83	1.43	0.41	0.64	72.28	1.93	0.75	1.24
	HYLAND	14.31	817.81	26.20	1.97	0.58	0.73	81.93	3.49	0.76	2.01
	LPJ_GUESS	14.31	817.81	31.70	1.82	0.69	0.73	66.84	2.32	0.62	1.64
	LPJ	14.31	817.81	32.17	2.12	0.63	0.91	64.55	2.82	0.69	1.82
	OCN	14.31	817.81	32.25	1.57	0.70	0.60	57.53	2.74	0.71	1.44
	ORCHIDEE	14.31	817.81	30.31	1.53	0.69	0.56	82.19	2.76	0.69	2.07
	TRIFFID	14.31	817.81	22.99	1.61	0.65	0.47	78.43	3.11	0.73	2.11
	VEGAS	14.31	817.81	35.37	1.22	0.69	0.53	60.48	1.29	0.63	0.89
MsTMIP	CLM4	14.31	817.81	22.96	2.46	0.50	0.88	54.01	1.49	0.76	0.71
	CLM4VIC	14.31	817.81	12.20	3.50	0.49	0.66	42.39	1.54	0.76	0.57
	DLEM	14.31	817.81	25.36	1.72	0.68	0.54	57.74	1.79	0.71	1.00
	GTEC	14.31	817.81	25.69	2.06	0.47	0.92	84.84	2.34	0.63	2.16
	ISAM	14.31	817.81	37.22	1.99	0.61	0.99	45.16	1.91	0.56	1.04
	ORCHIDEE-LSCE	14.31	817.81	26.83	2.99	0.54	1.24	61.57	3.95	0.61	2.38
	VEGAS2.1	14.31	817.81	34.29	1.47	0.74	0.56	61.92	1.26	0.61	0.92

886

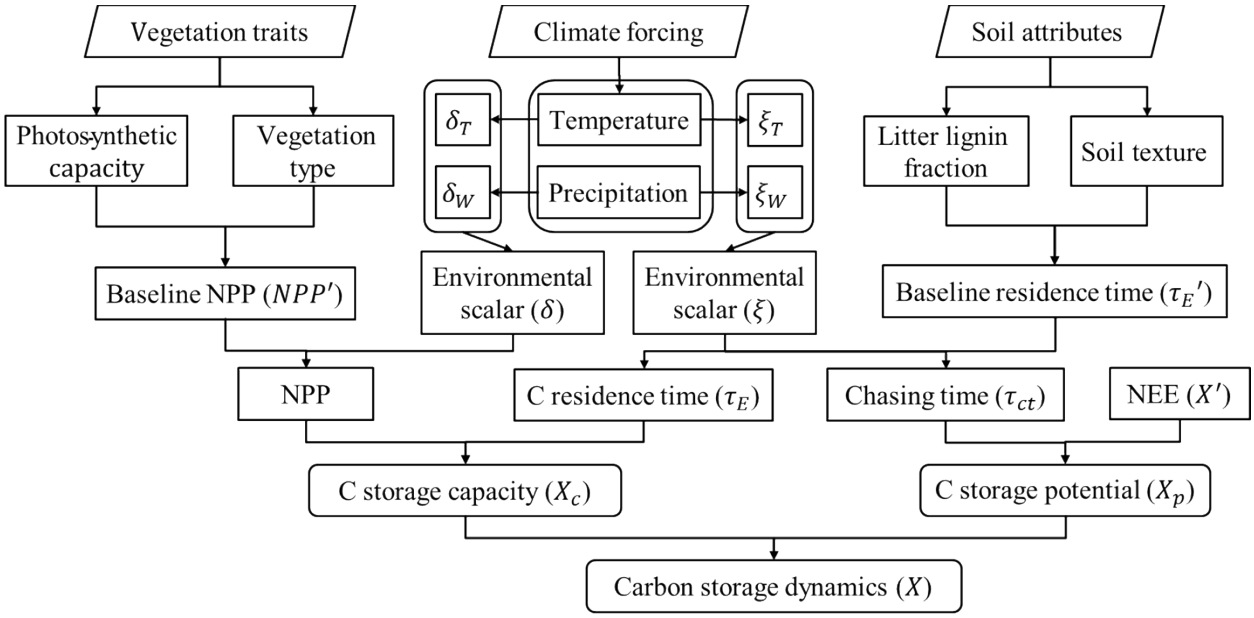

888

889 FIG. 1. Schematic diagram of the transient traceability framework. This framework traces the
890 modeled transient carbon storage dynamics to carbon residence time, NPP, carbon storage
891 potential, and their source factors.

892

893

894

895

(c)

(f)

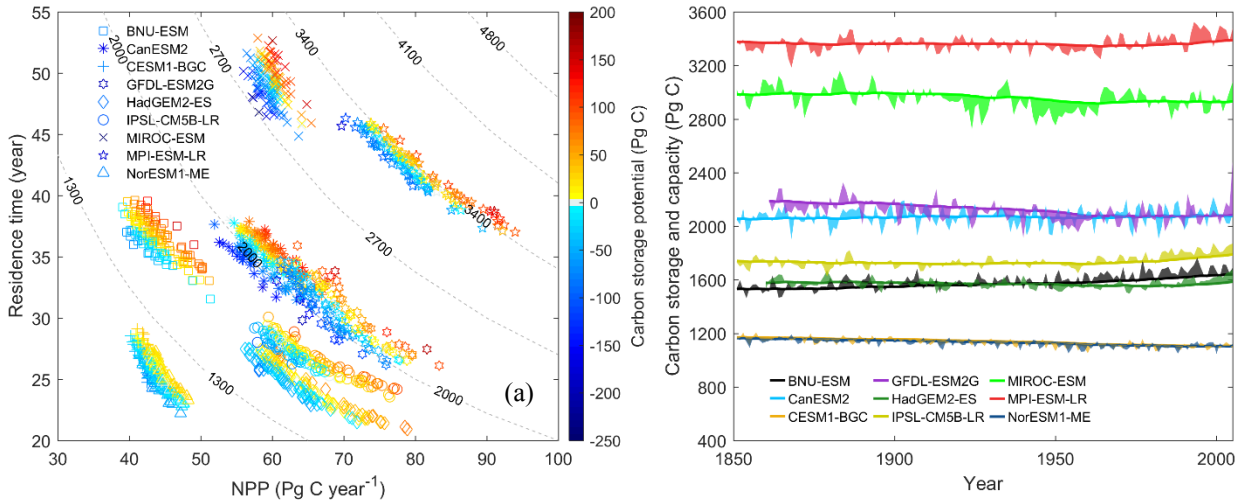
BNU-ESM
CanESM2
CESM1-BGC
GFDL-ESM2G
HadGEM2-ES
IPSL-CM5B-LR
MIROC-ESM
MPI-ESM-LR
NorESM1-ME
Residence time (year)
NPP (Pg C year-1)
Carbon storage potential (Pg C)
(a)
Carbon storage and capacity (Pg C)
Year
(d)

896

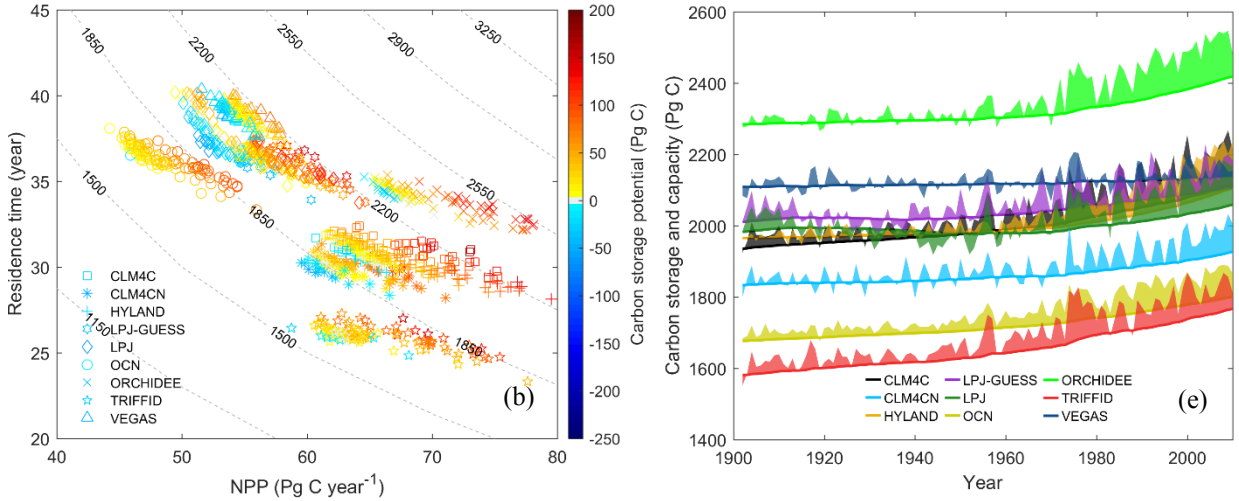
CLM4C
CLM4CN
HYLAND
LPJ-GUESS
LPJ
OCN
ORCHIDEE
TRIFFID
VEGAS
Residence time (year)
NPP (Pg C year-1)
Carbon storage potential (Pg C)
(b)
Carbon storage and capacity (Pg C)
Year
(e)

897

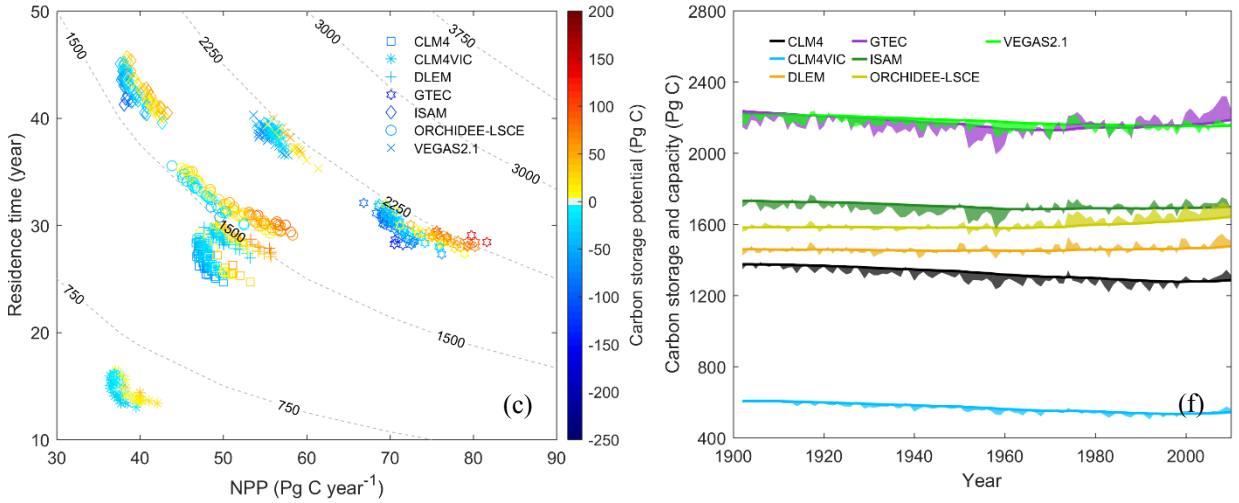
CLM4
CLM4VIC
DLEM
GTEC
ISAM
ORCHIDEE-LSCE
VEGAS2.1
Residence time (year)
NPP (Pg C year-1)
Carbon storage potential (Pg C)
(c)
Carbon storage and capacity (Pg C)
Year
(f)

898

900 FIG. 2. The 3D model output space (carbon residence time, NPP, and carbon storage potential),
901 and time series of annual carbon storage (solid line) with the shaded outline indicate the year-to-
902 year fluctuations due to changes in carbon storage capacity (in Pg C) for the models in (a, d)
903 CMIP5, (b, e) TRENDY, and (c, f) MsTMIP. The points in (a-c) represent the global annual
904 values for the three variables. The contour lines in (a-c) represent the carbon storage capacity.
905 The shades in (d-f) show the values of the carbon storage potential for the models (positive
906 above the solid lines, and negative below the solid lines).

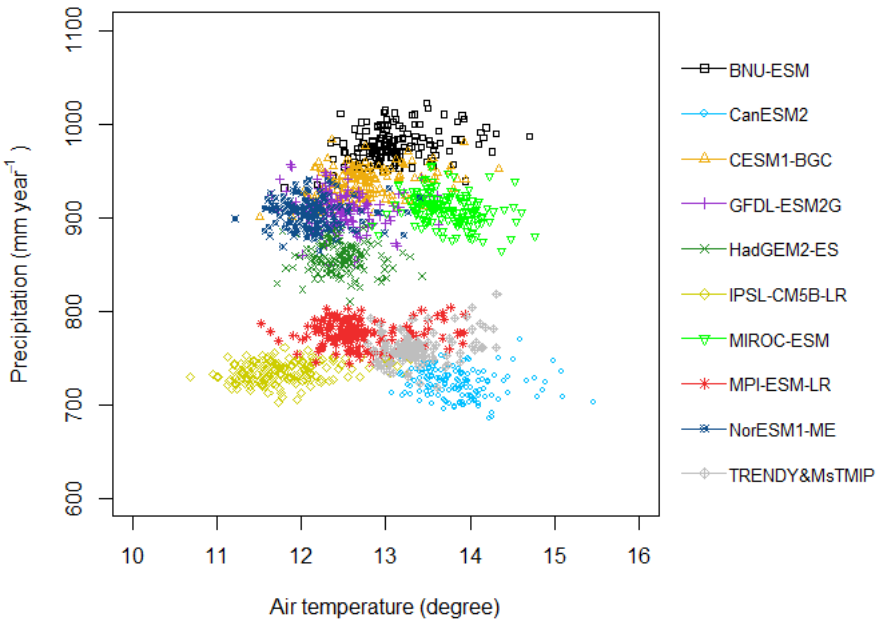

908

909 FIG. 3. Distribution of mean annual air temperature and total annual precipitation over land for
910 the nine ESMs in CMIP5, and the models in TRENDY and MsTMIP. The temperature and
911 precipitation are the same for the models in TRENDY and MsTMIP.

912

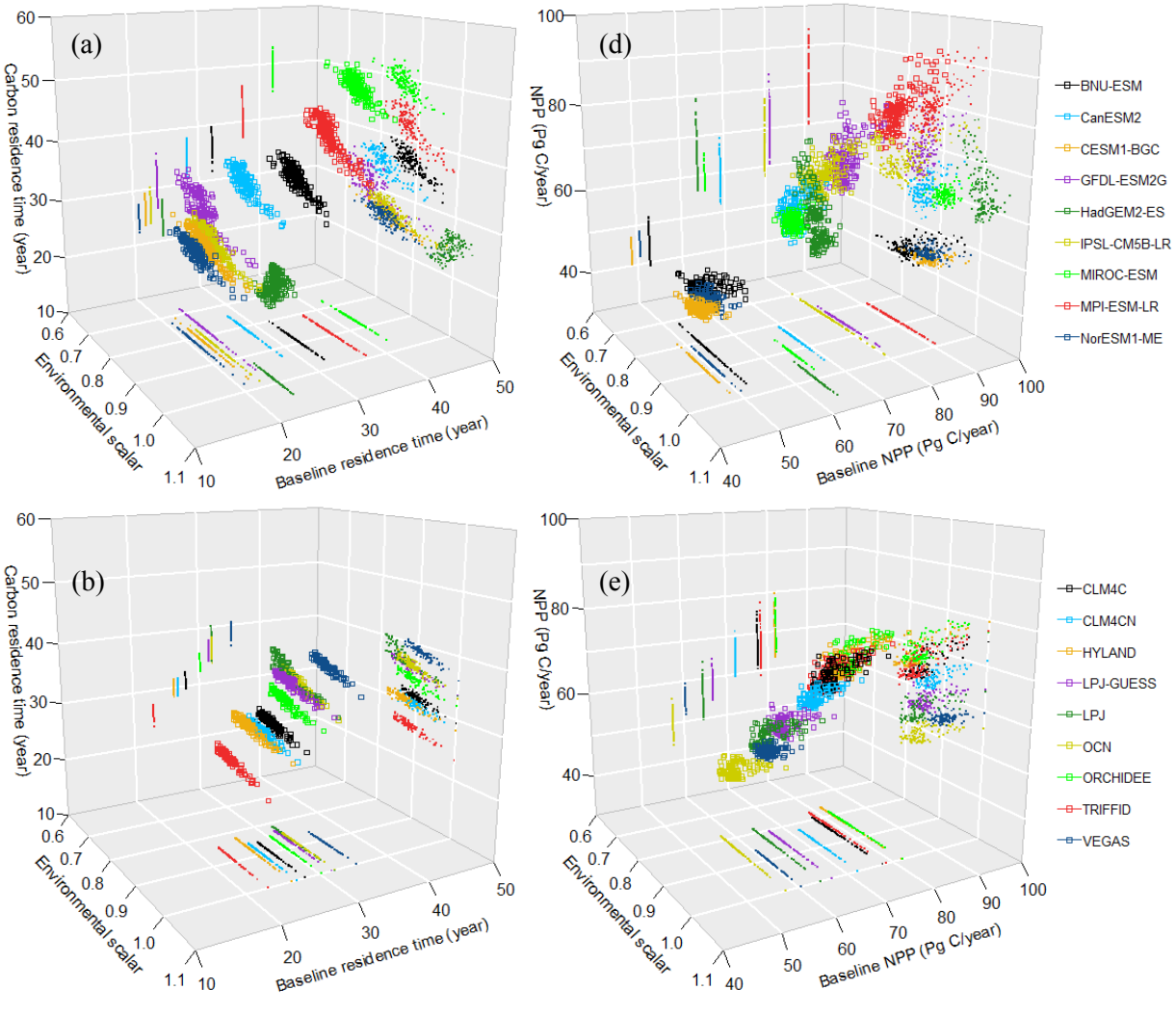
(a)
Carbon residence time (year)
Environmental scalar
Baseline residence time (year)
(d)
NPP (Pg C/year)
Baseline NPP (Pg C/year)
BNU-ESM
CanESM2
CESM1-BGC
GFDL-ESM2G
HadGEM2-ES
IPSL-CM5B-LR
MIROC-ESM
MPI-ESM-LR
NorESM1-ME
(b)
(e)
CLM4C
CLM4CN
HYLAND
LPJ-GUESS
LPJ
OCN
ORCHIDEE
TRIFFID
VEGAS

914

915

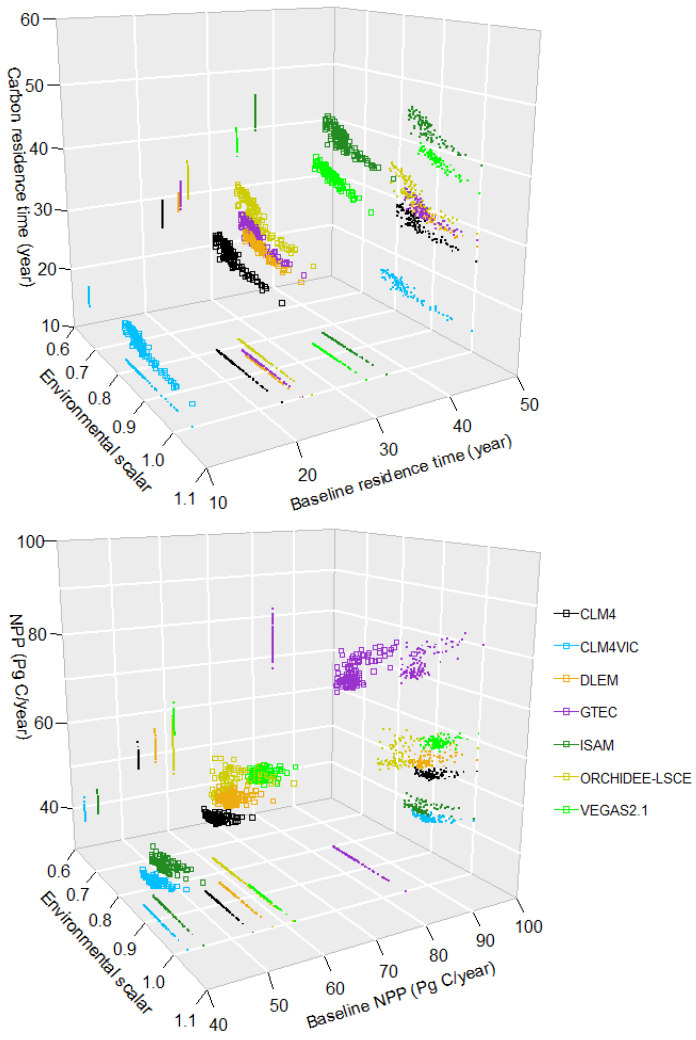

916

917

918 FIG. 4. Decomposition of the carbon residence time into the baseline carbon residence time and
(c) (f)
919 the environmental scalar, and decomposition of annual NPP into the baseline NPP and the
920 environmental scalar for (a, d) CMIP5, (b, e) TRENDY, and (c, f) MsTMIP. The environmental
921 scalar is a product of the temperature and water scalars, which convert the baseline carbon
922 residence time and baseline NPP into their actual values.

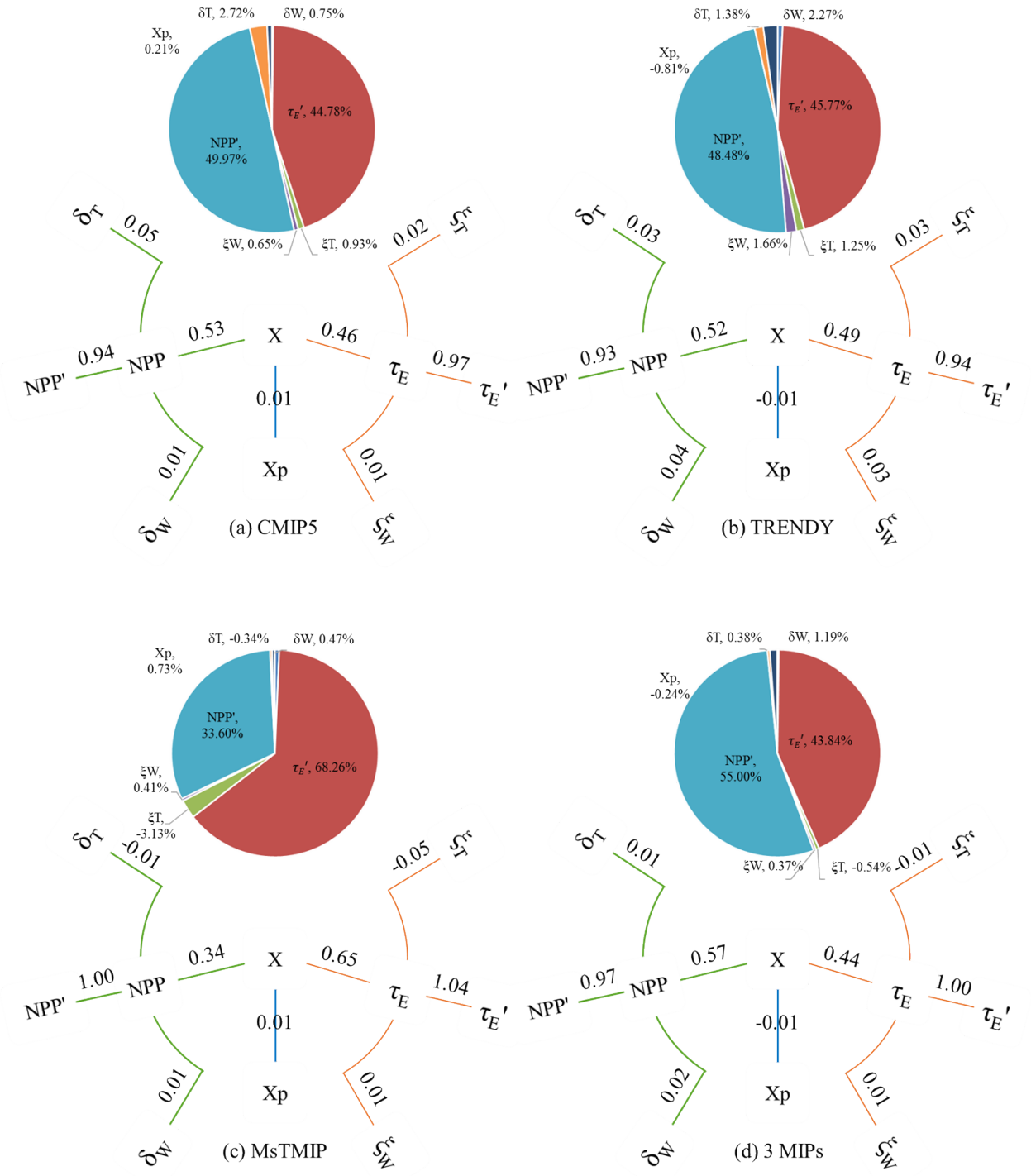

FIG. 5. Variance decomposition of the carbon storage based on global annual data from models in the three MIPs. First, the variation of the carbon storage (X) is decomposed into that of the carbon residence time (τ_E), NPP, and the carbon storage potential (X_p). Second, variations of the

carbon residence time and NPP are decomposed into their baseline values ($\tau_E^{'}$ and $NPP^{'}$) and the temperature (ξ_T and δ_T) and water (ξ_W and δ_W) scalars.

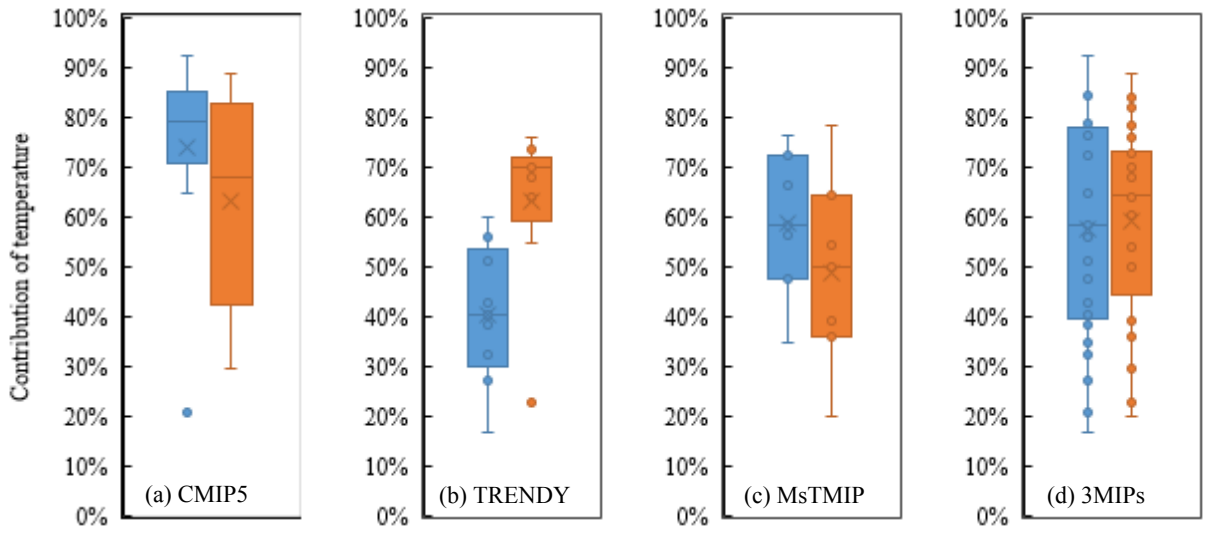

930

931 FIG. 6. Distribution of the temperature contributions to the variations in the carbon residence
932 time (blue box) and NPP (orange box) for (a) CMIP5, (b) TRENDY, (c) MsTMIP, and (d) the
933 three MIPs combined.